

Resonant microwave pulse compressor operating in two frequencies

L. Beilin, A. Shlapakovski, and Ya. E. Krasik
 Physics Department, Technion 32000 Haifa, Israel

(Received 1 May 2013; accepted 25 June 2013; published online 17 July 2013)

A resonant microwave pulse compressor with a hybrid (Magic) waveguide tee as an interference switch was studied in numerical simulations and experimentally. In this compressor, the necessary condition for energy storage in the compressor cavity is frequency-independent, so that its operation in different cavity eigenmodes without mechanical tuning is possible. An S-band compressor operating in two different frequencies (neighboring modes) was investigated. Two characteristic geometries corresponding to different regimes of the microwave energy accumulation and release were tested using input pulses of 200–400 kW power, 2.4 μ s duration, and variable frequency, 2.8 to 2.9 GHz. The geometries are characterized by an RF electric field in the interference switch that is higher or lower than the field in the cavity. The plasma discharge that switches the phases of compressor operation from energy storage to release was initiated by small metallic cones placed in the appropriate location. For both geometries, the nanosecond output pulses in two resonant frequencies were obtained; the maximal peak output power measured was \sim 1.8 MW. The efficiency of the microwave extraction was limited by either an insufficient coupling to the tee output arm (in the case of a high field in the tee) or non-uniformity of the plasma discharge (in the case of low field in the tee). © 2013 AIP Publishing LLC. [<http://dx.doi.org/10.1063/1.4813617>]

I. INTRODUCTION

Microwave pulse compressors are known to be successfully implemented for increasing the RF drive power in linear electron accelerators. The compressors currently in use on high-energy linear colliders¹ are intended to achieve the few-hundred-megawatt power levels using 50–100 MW klystrons.² In the SLED-II (SLAC Energy Development) system used at SLAC,² the compression method is based on the phase reverse of the input signal exciting short-ended delay lines. The power gain for this method is limited theoretically by the value of nine;² the SLED-II compressor used on the Next Linear Collider Test Accelerator (NLCTA) compresses a 50-MW, 1.5 μ s pulse with a power gain of \sim 4 at 80% efficiency.¹

For laboratory research, the method of resonant pulse compression is more appropriate as it can provide much higher power gains. The resonant pulse compression is a promising approach to high-power microwave generation^{3,4} since it allows one to produce microwave pulses of nanosecond duration and megawatt-to-gigawatt peak power using rather compact and relatively inexpensive pulsed microwave generators operating with a high repetition rate. In a resonant microwave compressor, the RF energy is stored in a high-Q cavity; then, a switch is activated to rapidly “open” the cavity, so that its Q-factor decreases drastically, and the energy is released into a load over a time interval much shorter than the time it takes to store it. Typically, a relative bandwidth of cavity resonance is $\sim 10^{-4}$; therefore, resonant pulse compressors are narrow-band devices and this limits their attractiveness as high-power microwave sources for laboratory research in which any frequency tuning is needed.

While the simplest way to change the operating frequency in resonant compressors is to adjust the device’s

geometry, it is of interest to provide frequency agility without mechanical tuning. This is possible for discrete frequency variation if a compressor is capable of operation in different (neighboring) cavity eigenmodes. In a recent work,⁵ such a possibility was considered for two compressor configurations. For the conventional, most frequently used configuration employing a waveguide H-plane tee as an interference switch^{3,4} (see Fig. 1(a)), the length of the shorted arm of the tee is normally adjusted to provide the equality of the cavity eigenfrequency and the closing frequency of the tee; therefore, for a transition to a different cavity mode, a geometry change is needed. It was shown in Ref. 5 that the transition to a neighboring mode is, nevertheless, possible without mechanical tuning if the tee is “sub-opened” to a certain degree. This means, however, that the same operation of the compressor in either frequency is achieved at the expense of the appearance of a prepulse and a reduced gain. Namely, it was demonstrated in experiments with the X-band compressor that the gain decreases by 5–6 dB as compared to the gain obtained at either of the two frequencies when the H-plane tee shorted arm length was mechanically adjusted.

Another option discussed in Ref. 5 is to use a symmetrical compressor configuration, based on a hybrid (Magic) waveguide tee. In this configuration, the H- and E-arms of the Magic-tee serve as the compressor input and output arms, and the collinear (side) arms are shorted, forming a storage cavity (see Fig. 1(b)). If the side arms are identical, there is no coupling to the output arm and the microwave energy is accumulated in the cavity. If the lengths of the side arms differ by a quarter guide wavelength, the stored energy is released. Such a symmetrical configuration was implemented in experiments on the compression of microwave pulses generated by a relativistic magnetron.⁶ It is important to emphasize that the necessary condition to build up a cavity

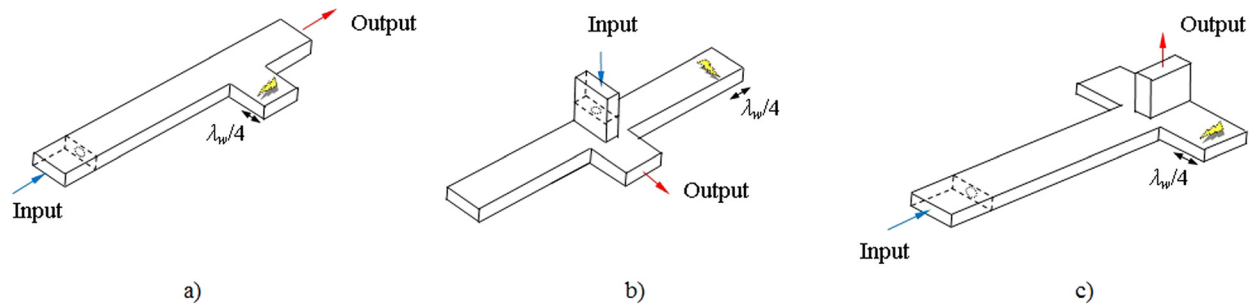


FIG. 1. Schematics of resonant microwave compressors appropriate for frequency tuning: (a) Conventional configuration with H-plane tee-based switch; (b) symmetrical storage cavity; (c) compressor with hybrid (Magic) tee-based switch.

resonance in this Magic-tee-based scheme is the symmetry of the system,⁷ which means frequency is not involved as in the configuration with the H-plane tee. Therefore, the scheme with a symmetrical storage cavity appears to be very suitable for application in a frequency-tunable compressor. The operating frequency can be varied continuously, with a mechanically changing cavity length (as was proposed also in Ref. 8), or discretely, using different cavity eigenmodes without mechanical adjustments. To the best of our knowledge, no experiments with a symmetrical microwave compressor demonstrating the frequency variation have yet been conducted.

In the present work, still another configuration of the frequency-agile microwave pulse compressor is considered. This compressor comprises a conventional, non-symmetrical storage cavity and the Magic-tee, with the symmetrical shorted side arms being the frequency-independent interference switch (see Fig. 1(c)). As compared to the symmetrical compressor, this scheme allows for operation at a larger number of discrete frequencies within a given frequency interval at a given cavity length. Indeed, the symmetrical storage cavity can be excited either only in symmetric modes or only in anti-symmetric modes, depending on which arm of the Magic-tee, the H- or E-arm, is used as the input arm. A compressor in which, for instance, the H-arm is the input arm cannot operate in the cavity eigenmodes with an even axial index, because the input coupling is realized via the RF electric field, which for these modes is zero in the symmetry plane. Similarly, if the input is through the Magic-tee E-arm, a compressor cannot operate in eigenmodes with an odd axial index. Unlike in the symmetrical compressor, in the scheme of Fig. 1(c), any cavity eigenmode can be operating and no mechanical tuning is required for the frequency variation. In addition, to achieve this, the tee “sub-opening” is not required, unlike in a conventional compressor (Fig. 1(a)); thus the prepulse level will be negligible at any frequency.

The goal of this work was to study the two-frequency S-band resonant compressor with the Magic-tee-based switch and, in particular, to demonstrate its operation at either of the two frequencies without mechanical tuning. The compressor was investigated in numerical simulations and experimentally at low and high microwave power. It should be noted that in both simulations and experiments, the simple geometry of the tee was studied; all its waveguides had a standard rectangular cross-section and there was no matching elements at the waveguide junctions. In fact, not a true Magic-tee but simply

the hybrid waveguide tee was used as the interference switch. The importance of appropriate matching was emphasized in Ref. 9; it will also be discussed below.

II. NUMERICAL SIMULATIONS: CAVITY CHARGING AND MICROWAVE EXTRACTION

The processes of microwave energy storage in and release from the compressor were simulated using the fully electromagnetic particle-in-cell (PIC)-code MAGIC.¹⁰ The simulation geometry is shown in Fig. 2; all its elements are rectangular waveguides of standard 72×34 mm cross-section. In all the simulations whose results are presented below, the material of the waveguide walls and input iris was brass (specific conductivity $\sigma = 1.56 \cdot 10^7 \Omega^{-1} \text{m}^{-1}$). The input iris had a fixed thickness of 4 mm and circular coupling hole, 27 mm in diameter filled with a dielectric having a permittivity $\epsilon = 2.25$. The position of the input iris was changed, determining the variable length of the cavity, L , which is the distance from the inner wall of the iris to the end wall in the tee. Also variable was the total length l of the two identical shorted side arms of the tee. In all simulations, the amplitude of the RF voltage applied to the input port in the fundamental TE_{10} mode was set the same (15 kV over the centerline across the waveguide). This corresponds to an input power of 210–220 kW, depending on the frequency. The frequency was varied to find a resonant value that would provide a maximal build-up of RF fields within the cavity and minimal reflection from the iris. The two neighboring eigenmodes having axial indices $n = 14$ and 15 (number of electric field variations in the standing wave pattern along the cavity) were considered.

In the simulations, different regimes of the energy storage and release were found. The energy storage regime is

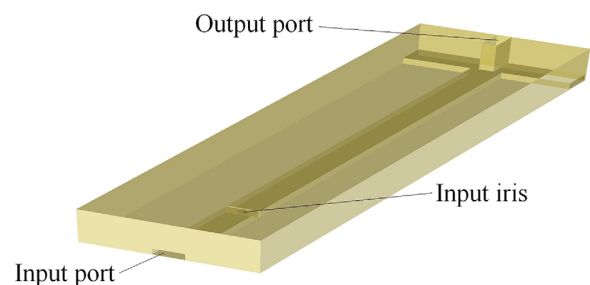


FIG. 2. 3-D view of the simulation region used in MAGIC-simulations.

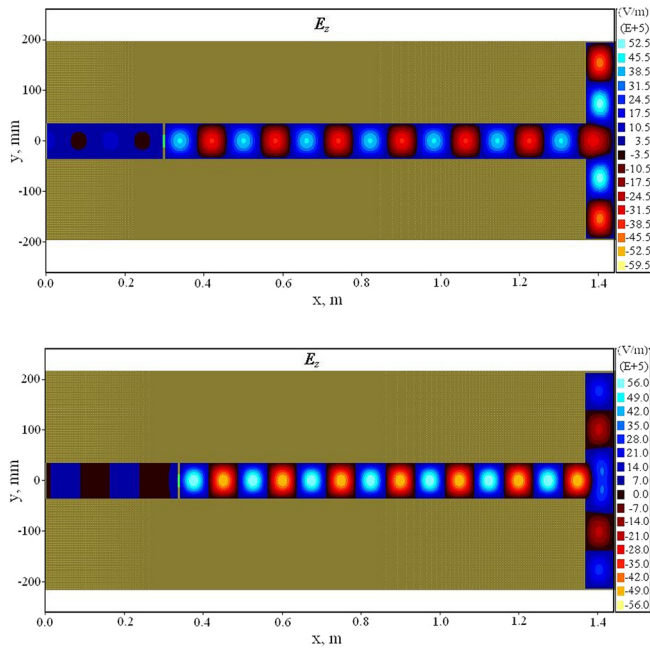


FIG. 3. Contour plots of the electric field for two characteristic geometries (x - y cross-section of the simulation region at the cavity center plane $z=0$). Geometry A (upper): $L=114$ cm; $l=39$ cm; $n=14$; $f_1=2.79$ GHz. Geometry B (lower): $L=110$ cm; $l=42.8$ cm; $n=15$; $f_2=2.8857$ GHz.

characterized by the RF electric field amplitude in the side arms, E_{side}^{max} , in comparison with that in the antinodes of the excited standing wave in the cavity, E_{cavity}^{max} . Namely, the ratio $R = E_{side}^{max}/E_{cavity}^{max}$ depends on the relationship between the length l and the half guide wavelength at the resonant frequency determined by both lengths L and l , i.e., the ratio R can differ for the frequencies of two neighboring eigenmodes f_1 and f_2 . Moreover, it can be considerably higher or significantly lower than unity, which is of crucial importance for ignition of a plasma discharge to activate the interference switch of the compressor. This is illustrated in Fig. 3, where the contour plots of the electric field are shown for two characteristic geometries, A and B, described below. In the upper plot, the highest electric field is in the side arms, so that it is easier to trigger the plasma discharge there, whereas in the lower plot, the electric field in the side arms is rather weak, which requires an initiation of the discharge that is reliable, so that a breakdown in the main cavity is avoided. However, a comparison of the cavity field in the upper and lower plots shows that in the lower plot it is higher, so that with appropriate triggering, one could obtain a higher output power for geometry B.

TABLE I. Characteristics of the cavity eigenmodes obtained in simulations.

	Geometry A: (highest E_{side} at f_1)		Geometry B: (low E_{side})	
	14	15	14	15
Eigenmode index	14	15	14	15
Eigenfrequency	$f_1 = 2.79$ GHz	$f_2 = 2.8558$ GHz	$f_1 = 2.7976$ GHz	$f_2 = 2.8857$ GHz
Max. E_{side}	58.5 kV/cm	48.6 kV/cm	29.1 kV/cm	24.9 kV/cm
Max. E_{cavity}	47.1 kV/cm	53.6 kV/cm	52.9 kV/cm	60.1 kV/cm
$R = E_{side}^{max}/E_{cavity}^{max}$	1.24	0.91	0.55	0.41
Cavity gain	14.6 dB	15.7 dB	15.6 dB	16.7 dB

The difference in the electric fields in the side arms can be explained if one considers the system as two coupled circuits: the long main cavity and the short cavity formed by the side arms. Then, the greater oscillatory energy is in the circuit whose “natural” frequency is nearer the resonant frequency of the system (normal mode frequency).¹¹ Since the spectrum of the system is, in general, much closer to a “natural” spectrum of a long cavity than to a rare spectrum of a short one, the field in the side arms, if it exceeds the field in the main cavity, can exceed it only slightly. In contrast, if the field in the side arms is weak, it can be much lower than the cavity field.

For different energy storage regimes, two characteristic geometries were chosen, which were then studied in simulations of energy release and tested experimentally. The results of the simulations of the cavity charging in the two eigenmodes for these geometries are summarized in Table I. Geometry A ($L=114$ cm, $l=39$ cm) provides a maximal possible ratio $R \approx 1.24$ for the eigenmode with $n=14$ (at the frequency f_1). In the neighboring mode ($n=15$, f_2), the field in the side arm is lower, but nevertheless sufficiently high. Geometry B preserves about the same eigenfrequency f_1 but features a significantly lower field in the side arms. The duration of the field build-up (simulation time) for the results presented in Table I was about $2.3 \mu\text{s}$. The cavity gain was calculated as the ratio of the power in the traveling wave component of the cavity field to the input power.

It is seen in Table I that in both geometries the difference in gain for neighboring eigenmodes is only ~ 1 dB, which seems quite acceptable for a compressor capable of operating in two frequencies. In addition, Table I presents numerically the results shown in Fig. 3. It should be noted that the electric field in the side arms for geometry B is even less than the breakdown threshold for air at atmospheric pressure. On the other hand, the gain at the highest side arm field (geometry A, frequency f_1) is ~ 2 dB lower than in the opposite case (geometry B, frequency f_2), which is rather significant.

For the microwave energy extraction, the characteristic of the regime is the power transmission from the input, H-arm, to the output, E-arm, when the lengths of the shorted arms differ from each other by a quarter guide wavelength $\lambda_w/4$. An ideally matched Magic-tee would provide full transmission in this case, regardless of the frequency and length of the shorted arms. However, for simple geometry without matching elements, the transmission significantly depends on the frequency and side arm length. This was demonstrated in simulations, in which the input iris was

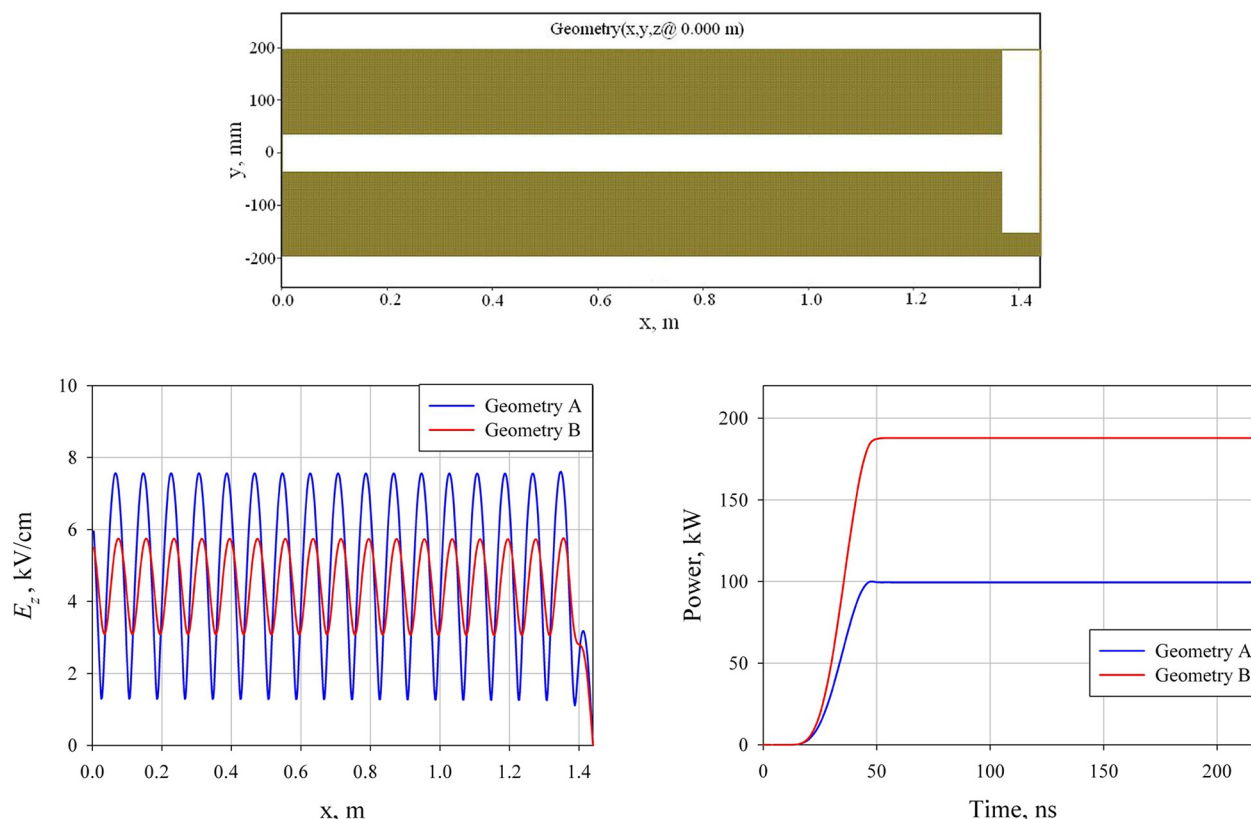


FIG. 4. Microwave transmission with side-arm lengths differed by the quarter guide wavelength. Top: simulation region cross-section at the cavity center plane ($z = 0$). Bottom: Standing wave pattern in the H-arm (left) and output power in the E-arm (right). Frequency is 2.8 GHz, input power is ≈ 210 kW.

absent and the side arm lengths were $l/2$ and $l/2 - \lambda_w/4$ (see Fig. 4) with $l = 39$ cm and 42.8 cm (geometries A and B).

In the lower plots of Fig. 4, the absolute value of the RF electric field at the waveguide centerline averaged over the oscillation period and the power at the output port (see Fig. 2) are shown. These plots were obtained for the frequency of 2.8 GHz close to the eigenfrequency f_1 for geometries A and B. It is seen that, for geometry A, the standing wave pattern in the H-arm exhibits a rather high standing wave ratio (SWR) showing a significant reflection and the power at the output port is only ~ 100 kW, so that the transmission into the E-arm is $\leq 50\%$. Meanwhile, for geometry B at the same frequency, the SWR is low and the transmission into the E-arm is about 90%. Thus, a geometry that provides a higher electric field in the side arms in the energy storage mode (identical side arms) does not provide a proper output coupling of the cavity in the energy release mode (side arm lengths differed by $\lambda_w/4$). In contrast, a geometry that provides almost full output coupling in the energy release mode is characterized by a lower electric field in the side arms in the energy storage mode.

The process of extracting the accumulated microwave energy from the cavity was modeled using the IONIZATION command available in the MAGIC code. The simulations started from the preset RF fields, which were obtained in the simulations of the cavity charging, and then, the ionization was turned on within the 4-mm thick layer crossing the side arm waveguide at the location of the electric field maximum (see Fig. 5). The rate of ionization was set equal to $5 \cdot 10^{12} \text{ cm}^{-3}$ per nanosecond; the duration of the ionization

process was 1.3 ns; the background gas was nitrogen at atmospheric pressure. The ions of the produced plasma were considered immobile, and the dynamics of electrons was determined by the existing RF electric field and collisions with neutrals as realized in the MAGIC code. Due to the frequent electron-neutral interaction at atmospheric pressure, the electrons acquire kinetic energy of the order of only tens of eV after the start of ionization. An example of the phase space for electrons obtained at a 0.6 ns time delay with respect to the beginning of the ionization is presented in Fig. 5. After the end of ionization, the phase space rapidly becomes uniform, with only a small amount of particles having energy in excess of 20 eV. It is understood that this model is not self-consistent, as the ionization is set artificially. Nevertheless, the E_z field at the plasma boundary rapidly decreases down to almost zero, thus simulating the appearance of a reflector at the quarter guide wavelength from the wall; one can therefore consider that the model describes the process of energy release satisfactorily.

The power at the output port obtained in these simulations is shown versus time in Fig. 6 for geometries A and B at both resonant frequencies, f_1 and f_2 . It is seen that the process of energy release differs for different regimes rather significantly. For geometry A, which is characterized by a strong field in the side arms at the energy storage stage, there is first a short peak in the output power, whose duration corresponds to the wave double transit along one side arm, and then the longer lower-power part follows, in steps of cavity double transit duration. In fact, when the plasma produced

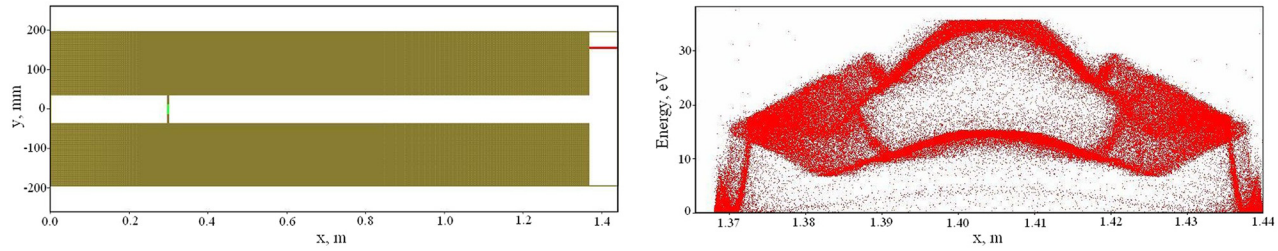


FIG. 5. Configuration and phase portraits of particles. Left: x - y plane at $z=0$ (cavity center plane). Right: kinetic energy vs. x at 0.6 ns after the beginning of the ionization. Geometry A, frequency $f_1 = 2.79$ GHz.

by the IONIZATION command causes the side arms to differ in length by $\sim \lambda_w/4$, the energy from the cavity main part is extracted in portions due to a low, $\sim 50\%$, cavity-to-output transmission coefficient (see Fig. 4). The peak is higher for frequency f_1 since the stored side arm field is higher in f_1 than in f_2 (Table I). The “flat” part is higher for frequency f_2 due to both the higher stored cavity field and larger transmission from the cavity into the output arm. It should be noted that, for instance, for frequency f_1 , the power in the traveling wave component of the stored cavity field before switching is ~ 5.6 MW, while the output power in the “flat” part is only 2.3–2.4 MW. This means that the output power in the “flat” part is even less than that determined by $\sim 50\%$ cavity output coupling, i.e., there are additional power losses in the produced plasma.

For geometry B, in contrast, the field stored in the side arms is rather weak, and therefore, the first short peak is only slightly manifested at frequency f_1 and totally absent at frequency f_2 . The output power is considerably higher than the power in the “flat” part of the curves in the case of geometry A, due to both the higher cavity gain and larger transmission into the output arm. At frequency f_1 in geometry B, in which the transmission is $\sim 90\%$ (see Fig. 4), almost all the energy is released for the cavity double transit time; at frequency f_2 , there is a considerable “tail” in the output power pulse due to larger reflections. Nevertheless, the power in the main part of the pulse is slightly higher than that at frequency f_1 because of a higher cavity gain. In addition, at both

frequencies, the output power is less than the power of the traveling wave component of the cavity field before switching; thus, there are losses in the plasma as well.

III. EXPERIMENTAL RESULTS

The features of these two characteristic geometries were tested experimentally using the setup shown in Fig. 7. The rectangular waveguide compressor cavity of the WR284 cross-section with the iris at its input end was connected at the output end to the H-arm of the Magic-tee. Identical waveguide sections shorted with copper membranes were connected to the Magic-tee side arms. Two pairs of sections having different lengths were used to arrange geometries A and B, and different waveguide spacers provided the proper cavity lengths. The main part of the cavity was the 40 dB directional coupler, so that the power of the traveling wave component of the cavity field could be easily measured.

The resonant frequencies of the two neighboring modes of the system measured with an R&S ZVL network analyzer were $f_1 = 2801.0$ MHz, $f_2 = 2866.0$ MHz for geometry A and $f_1 = 2801.2$ MHz, $f_2 = 2891.6$ MHz for geometry B (at $\sim 2 \cdot 10^5$ Pa pressure of dry air inside the system), which is in satisfactory agreement with the resonant frequencies found in simulations. The cavity gain at both frequencies in both geometries also agreed well with the simulation results (see Table I). The RF field in both side arms was measured using B-dots at the waveguide narrow wall at a distance of

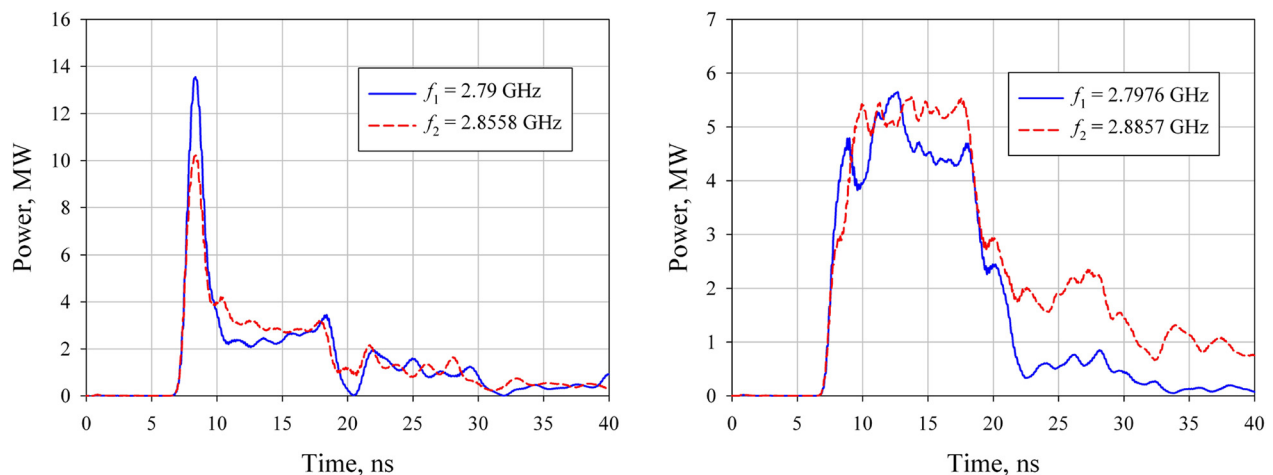


FIG. 6. Time dependences of the output power from MAGIC simulations with the IONIZATION command for geometries A (left) and B (right). The input power corresponds to 15 kV RF voltage over the centerline across the waveguide (≈ 210 kW for frequencies f_1 and ≈ 220 kW for f_2).

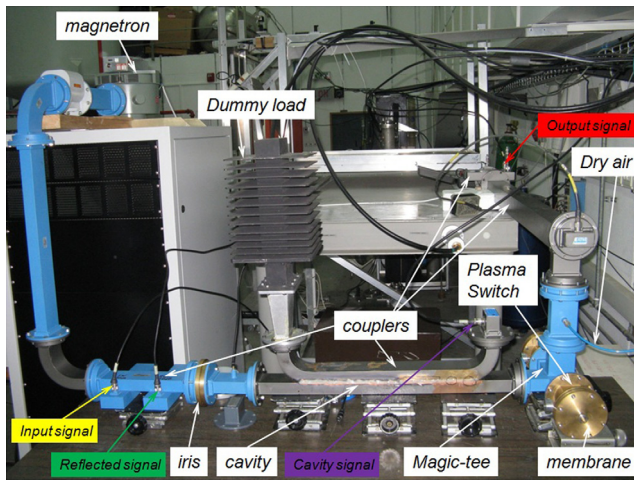


FIG. 7. Microwave pulse compressor with the hybrid (Magic) tee-based interference switch.

40 mm ($\approx \lambda_w/4$) from the membranes. The results of these measurements also agreed with the simulation results. The degree of the tee side arms' identicalness was sufficient to provide a transmission coefficient S_{21} from the cavity input to output of lower than -42 dB at both resonant frequencies in both geometries.

To measure the cavity-to-output transmission in the case of a $\approx \lambda_w/4$ difference in the side arm lengths, a waveguide section with a sliding short was connected to the Magic-tee instead of one section with the membrane. The results of these measurements with sections corresponding to geometries A and B are shown in Fig. 8 (the difference in the shorted arms' length was 40 mm in both cases; the input signal was applied to the H-arm without the iris). It is seen that for geometry A, the transmission at both resonant frequencies (2801 and 2866 MHz) is < -5 dB, which is even less than the $\sim 50\%$ obtained in the simulations. Meanwhile, for geometry B, the transmission at frequency $f_1 = 2801.2$ MHz is almost full, in good agreement with the simulations. At frequency $f_2 = 2891.6$ MHz, the transmission is as low as ≈ -4.5 dB. Such a low transmission must lead to the output power for the compressor based on the tee with non-matched H- and E-arms being significantly limited.

The compressor was charged by a frequency-tunable CPI VMS1177 magnetron generating input pulses of 200 to 400 kW power at up to $2.5 \mu\text{s}$ duration. With regard to the energy storage stage, experiments with the magnetron also

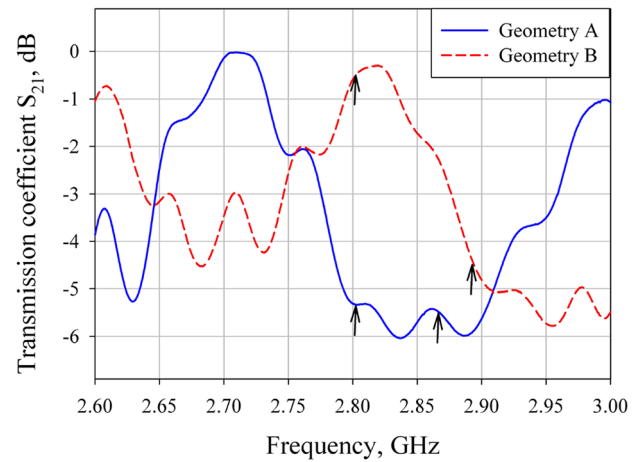


FIG. 8. Transmission from the tee H- to E-arm measured with the network analyzer when the shorted side arms differed in length by 40 mm. Arrows indicate resonant frequencies for geometries A and B.

confirmed the simulation results at a high power level. The measured prepulse power related to the input power was the same as the low-power measurements using the network analyzer. For the energy release, the plasma discharge was triggered and output pulses were obtained in the self-breakdown mode initiated by small copper and tungsten cones. A cone was attached to the wide wall of the waveguide, at a distance of 40 mm from the membrane in the side arm to trigger plasma formation at that location (see Fig. 9). It has been shown that with a given cone, a higher cavity field (magnetron power) is required to trigger the plasma discharge at frequencies f_2 than at frequencies f_1 in both geometries A and B. With cones having an insufficiently sharp apex, it was even impossible to obtain output pulses at frequencies f_2 since a breakdown occurred within the cavity because of insufficient field amplification in the side arm. This is in agreement with the simulations and B-dot measurements performed at low power. Accordingly, a longer or sharper cone providing stronger field amplification was used to trigger the discharge in geometry B than in geometry A.

The peak output power at the two operating frequencies in both geometries was of the same order of magnitude. At a certain cone (different for geometries A and B), no adjustment in addition to tuning the magnetron was needed to switch between the operating frequencies. The typical oscilloscope traces registered in the experiments are shown in Fig. 10. The behavior of the reflected signal corresponding



FIG. 9. Cone electrodes used to initiate the plasma discharge in the Magic-tee side-arm.

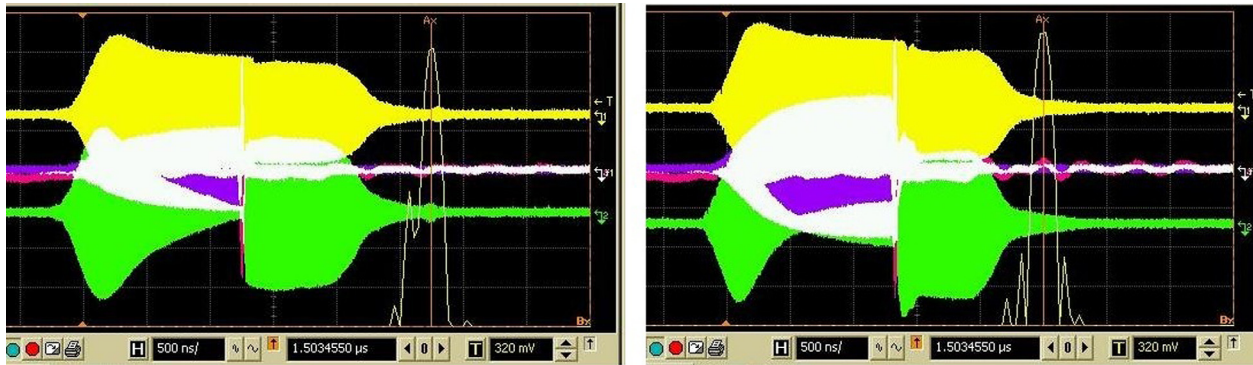


FIG. 10. RF voltages of the input (yellow), reflected (green), cavity (violet/white), and output (pink/white) signals. The frequency is 2801 MHz (left) and 2866 MHz (right). Geometry A. The time scale is 500 ns/div.

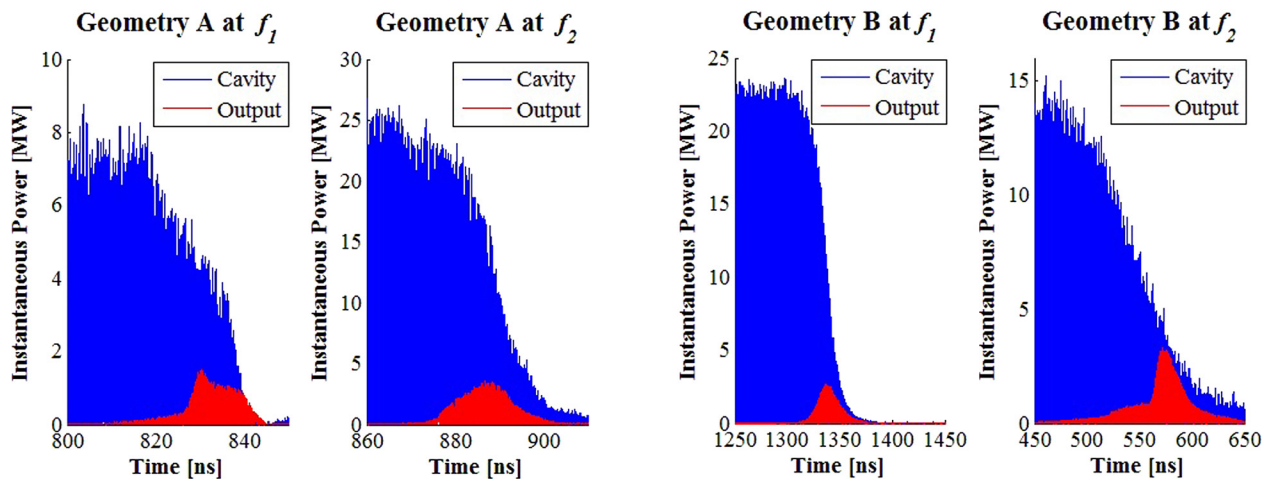


FIG. 11. Instantaneous power of the output and cavity signals for both resonant frequencies in the two geometries. Left: geometry A, copper cone of 3 mm length and 0.4 mm apex diameter. Right: geometry B, different tungsten cones (1.1 mm apex diameter; 5 mm length for f_1 and 7 mm for f_2).

to the cavity charging is clearly seen, as well as the field build-up in the cavity. In the nanosecond time scale, the calculated instantaneous power of some output signals together with signals delivered from the cavity via the 40 dB coupler is presented in Fig. 11.

The power averaged over the oscillation period can be estimated to be half of the instantaneous power. In Fig. 11, the plots presented for the two operating frequencies in the case of geometry A were obtained using the same cone electrode for discharge initiation; in the case of geometry B, the plots for the two frequencies were obtained using different initiators. The maximal peak output power achieved was ~ 1.8 MW at 2866 MHz in geometry A (shown in Fig. 11, left). The output power obtained with this cone at 2801 MHz was ~ 0.8 MW at an almost two times lower input power. Increasing the magnetron power at 2801 MHz resulted in a premature (earlier) breakdown, so that the power accumulated in the cavity (and the output power) did not increase. The maximum of ~ 1.6 MW in the output power at 2801 MHz was achieved with a cone 1 mm in length, which was insufficient to initiate the discharge at 2866 MHz (let us recall that the highest RF field in the side arms is in geometry A at 2801 MHz). The efficiency of power extraction (defined as the ratio of the peak

output power to the power of the traveling wave component of the cavity field) was for geometry A in the range of 13–17%. It should be noted that the short peaks obtained in the simulations (Fig. 6, left) were not registered. This can be explained by the plasma taking a longer time to be formed as compared to the time set in the simulations, as one can see from the slow rise of the output power in Fig. 11, left.

With geometry B, the same tendencies in the output at operating frequencies f_1 and f_2 were observed. The peak output power obtained with different cones was in the range of 1.3–1.7 MW. The maximal efficiency of power extraction reached $\sim 20\%$ at $f_2 = 2891.6$ MHz, whereas at $f_1 = 2801.2$ MHz it reached $\sim 11\%$ (Fig. 11, right). Moreover, at 2891.6 MHz, a rather high efficiency of energy extraction (defined as the output pulse energy divided by the energy stored in the cavity), $\sim 70\%$, was obtained due to the longer output pulse duration (the right plot in Fig. 11). It is important to note that for geometry B, the difference between the output power obtained in simulations and experiments is bigger than for geometry A (meaning the “flat” part of the output pulses shown in Fig. 6, left). This is a consequence of a much lower field in the side arms, which could result in slower and non-uniform plasma formation.

IV. CONCLUSIONS

A resonant microwave pulse compressor capable of discrete frequency variation without mechanical tuning was studied. This capability is achieved by using the hybrid (Magic) tee as a potentially frequency-independent interference switch. The generation of the output pulses in two S-band operating frequencies was demonstrated. The output pulses of 0.8–1.8 MW peak power were obtained at an input power of 200–400 kW; the FWHM pulse duration was 11 to 25 ns. Unlike in the first demonstration of changing operating frequency without mechanical tuning in the X-band compressor with the H-plane tee,⁵ the compressor operated in both frequencies with a negligible prepulse level.

It has been shown that the RF electric field magnitude in the Magic-tee side-arms at the energy storage stage is very sensitive to the geometry and is different (in a general case) for the two frequencies. Two characteristic geometries were investigated. In the configuration with a high field in the side arms (geometry A), the efficiency of the energy release is limited due to the system electrostatics, i.e., the cavity-to-output transmission after switching is rather low. The situation in this case can be improved by means of proper matching of the Magic-tee H- and E-arms, so that almost full transmission is provided. In the configuration with a low electric field in the side arms (geometry B), the efficiency of the energy extraction was limited due to the non-uniformity of the plasma discharge produced with the use of cone electrodes for discharge initiation. In this case, the situation can be improved if one implements other methods to trigger the discharge, such as laser triggering or using discharge tubes for high-voltage triggering at a pressure lower than that in the cavity volume.

ACKNOWLEDGMENTS

This work was partially supported by the Technion Grant No. 2013371 and by the Center for Absorption in Science, Ministry of Immigrant Absorption, State of Israel. The authors are thankful to Dr. A. Sayapin, Dr. Y. Hadas, and Dr. S. Artemenko for their interest, support, and fruitful discussions and A. Levin for technical assistance.

¹S. H. Gold and G. S. Nusinovich, "Review of high-power microwave source research," *Rev. Sci. Instrum.* **68**, 3945 (1997).

²C. Nantista, Z. D. Farkas, N. M. Kroll *et al.*, "High power RF compression with SLED-II at SLAC," *Particle Accelerator Conference (PAC 93)*, Washington, DC, May 17–20, 1993. SLAC-PUB-6145, April 1993.

³J. Benford, J. A. Swegle, and E. Schamiloglu, *High Power Microwaves*, 2nd ed. (Taylor & Francis, New York, London, 2007).

⁴A. N. Didenko and Yu. G. Yushkov, *Powerful Microwave Pulses of Nanosecond Duration* (EnergoAtomizdat, Moscow, 1984) (in Russian).

⁵V. A. Avgustinovich, S. N. Artemenko, and A. S. Shlapakovski, "Resonant frequency-tunable microwave compressors," *J. Commun. Tech. Electron.* **54**, 721 (2009).

⁶A. N. Didenko, I. I. Vintzenko, A. I. Mashchenko *et al.*, "The resonant compression of microwave pulses at the output of a relativistic magnetron," *Dokl. Phys.* **44**(6), 344–346 (1999).

⁷C. E. Baum, "Compression of sinusoidal pulses for high-power microwaves," *Circuit and Electromagnetic System Design Notes*, Note 48, March 2004.

⁸E. G. Farr, L. H. Bowen, W. D. Prather, and C. E. Baum, "Microwave pulse compression experiments at low and high power," *Circuit and Electromagnetic System Design Notes*, Note 63, January 2010.

⁹C. E. Baum, "Impedance-matched Magic tee," *Circuit and Electromagnetic System Design Notes*, Note 51, March 2006.

¹⁰B. Goplen, L. Ludeking, D. Smithe, and G. Warren, "User configurable MAGIC code for electromagnetic PIC calculations," *Comput. Phys. Commun.* **87**(1/2), 54–86 (1995).

¹¹A. B. Pippard, *The Physics of Vibrations, Omnibus Edition* (Cambridge University Press, New York, 1989), p. 368.